Fingered growth in channel geometry: A Loewner-equation approach

T. Gubiec[1] and P. Szymczak[2]
[1]*Institute of Experimental Physics, Faculty of Physics, Warsaw University, Hoża 69, 00-681 Warsaw, Poland*
[2]*Institute of Theoretical Physics, Faculty of Physics, Warsaw University, Hoża 69, 00-681 Warsaw, Poland*
(Received 8 January 2008; published 14 April 2008)

A simple model of Laplacian growth is considered, in which the growth takes place only at the tips of long, thin fingers. Following Carleson and Makarov [L. Carleson and N. Makarov, J. Anal. Math. **87**, 103 (2002)], the evolution of the fingers is studied with use of the deterministic Loewner equation. The method is then extended to study the growth in a linear channel with reflecting sidewalls. One- and two-finger solutions are found and analyzed. It turns out that the presence of the walls has a significant influence on the shapes of the fingers and the dynamics of the screening process, in which longer fingers suppress the growth of the shorter ones.

DOI: 10.1103/PhysRevE.77.041602 PACS number(s): 68.70.+w, 05.65.+b, 61.43.Hv, 47.54.−r

I. INTRODUCTION

A variety of natural growth processes, including electrodeposition, viscous fingering, solidification, dielectric breakdown or even growth of bacterial colonies can be modeled in terms of Laplacian growth. In this model a plane interface between two phases moves with velocity driven by a scalar field $u(\mathbf{r},t)$, which can represent e.g., temperature, pressure, or concentration, depending on the problem studied. The field satisfies the Laplace equation

$$\nabla^2 u(\mathbf{r},t) = 0, \tag{1}$$

with the boundary condition $u(\mathbf{r},t)=0$ at the phase interface. The normal velocity of the growing phase is proportional to the field gradient at the interface [or to some power (η) of the gradient]

$$v \sim |\nabla u(\mathbf{r},t)|^{\eta}. \tag{2}$$

An important property of Laplacian growth processes is the Mullins-Sekerka instability of the advancing interface. The field gradient over a small bump is larger than that over the plane interface, thus, for $\eta>0$, the bump grows faster than adjacent areas of the interface and develops into a finger. Contrastingly, for $\eta<0$, the bumps are flattened and the growth is stable.

Initial phases of the evolution of a plane interface are well understood in terms of linear stability analysis, which yields the wavelength of the most unstable perturbation [1,2]. However, the later stages of the evolution are no longer linear and hard to tackle analytically. Here we consider a simplified model of the developed nonlinear state: it is assumed that, as a result of the initial instability of the front, a number of fingerlike protrusions were formed. The further growth of the fingers is assumed to take place only at their tips (see Fig. 1), with velocities proportional to the field gradient. The dynamics is deterministic: once the initial geometry is given, the state of the system at any later time is uniquely determined. Thus, this model can be used when, except for the initial instability leading to the finger formation, the role of the noise in the evolution of the system can be neglected. Additionally, we neglect another noise-driven phenomenon: the tip-splitting effect when the single finger bifurcates into two or more daughter branches.

The above model of finger growth was formulated mathematically by Carleson and Makarov [4] (see also Selander's thesis [5]) and called by them "the geodesic Laplacian path model." Independently, a similar idea was considered by Hastings in [6].

In several experimental and numerical studies the patterns relevant to the above-introduced model have been observed. The examples include dendritic growth in some of the electrochemical deposition experiments [2,7], channeling in dissolving rocks [8], side-branches growth in crystallization [9], or fiber and microtubule growth [10]. Among the most beautiful experiments on the fingered growth are the combustion studies by Zik, Olami, and Moses [3,11]. In those experiments (some of the results of which are reproduced in Figs. 1 and 2) a solid fuel is burnt in a Hele-Shaw cell, i.e., in the narrow gap between two parallel plates. Near the flame ex-

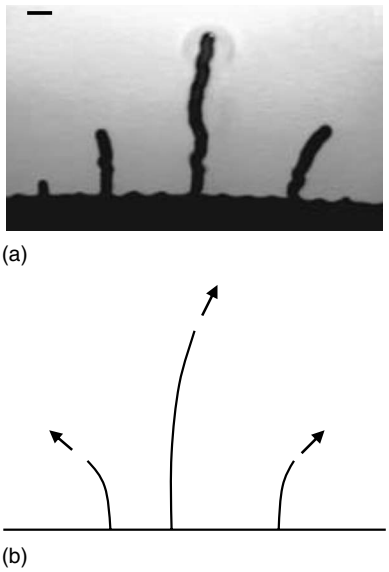

FIG. 1. Fingering in the combustion experiments [3] and the theoretical model (bottom). The scale bar corresponds to 1 cm. (The photograph is reproduced from [3].)

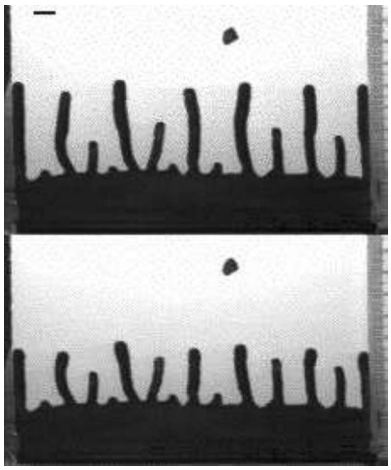

FIG. 2. Competition in the fingered growth in combustion experiments [3]. Initially equal sized fingers (bottom) evolve toward a state where every other finger stops growing (top). The scale bar corresponds to 1 cm.

tinction, as the flux of the oxygen supplied to the system is being lowered the initial instability of the combustion front develops into the sparse fingers (cf. Fig. 1), which appear to evolve in a regular or near-regular way. Similar fingered patterns are also observed in reverse filtration combustion in porous media [12]. For the "thin" finger model to be applicable, the width of the fingers should be much smaller than the separation between them. The concrete form of this condition depends on the problem studied—e.g., for the combustion problem this corresponds to the low Péclet number regime [3] (i.e., dominant diffusion in the transport equation).

Growth of the fingers demonstrates analogous instabilities as the plane front, since the gradients around the tips of the longer fingers are larger than those around shorter fingers. This leads to the so-called "shadowing effect"—the longer fingers grow faster and suppress the growth of the shorter ones in their neighborhood, which in some cases gives rise to a scale-invariant distribution of finger lengths [8,13]. Figures 2 and 3 present examples of such a competitive growth in the channeling processes in dissolving rock and in the combustion experiments described above.

In the absence of tip splitting, the number of competing fingers eventually decreases and finally a single finger survives the competition and persists to advance, in analogy with viscous fingering in a Hele-Shaw cell [14]. However, in a number of more complex growth problems (e.g., in directional solidification), the growth of the fingers ceases to be Laplacian in late stages of competition process, as the average distance between the surviving fingers increases. In such cases, the final steady state of the system may correspond to the multifinger array [15].

Most of the experiments on nonequilibrium growth mentioned above were performed in a quasi-two-dimensional (2D) geometry. A convenient way of solving the Laplace equation in two dimensions is to use a conformal mapping which transforms a domain under consideration to some simpler region where the solution may easily be found. A remarkable idea, due to Loewner [16], is to trace the evolution of the mapping instead of the evolution of the boundary itself. It turns out, namely, that the evolution of the map may be in many cases described by the first order ordinary differential equation (Loewner equation), which represents a considerable simplification in comparison to the partial differential equation describing boundary evolution. Loewner evolutions are intensely studied in the theory of univalent functions (for general references, see the monographs [17] and for a recent physical introduction see [18,19]). The subject has recently attracted a lot of attention in the statistical physics community in the context of stochastic Loewner evolution (SLE), which has proved to be an important tool in the study of two-dimensional critical systems [20].

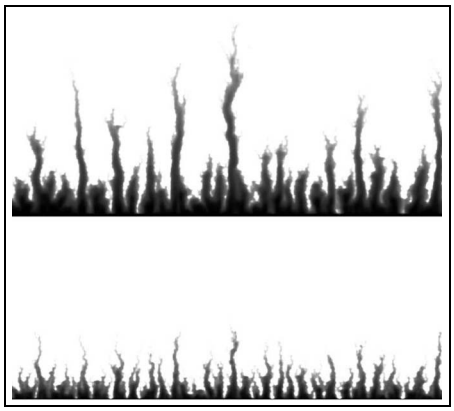

FIG. 3. Competitive dynamics of the channels in the dissolving rock fracture. The figures present the dissolution patterns at two different time points. Similar to Fig. 2, longer channels grow faster and suppress the growth of the shorter ones [8].

The exact form of the Loewner equation depends on the shape of the domain in which the growth takes place. Usually, it is either the complex half-plane (where the initial phase boundary corresponds to the real axis) or radial geometry (where the initial boundary is the unit circle in the complex plane). However, many experiments on the unstable growth are conducted in a channel geometry, between two reflecting walls. In this paper we show how to extend the Carleson and Makarov model to such a geometry. Using conformal mapping formalism we derive a Loewner equation for that case, which allows us to find the dynamics of the fingers and analyze the shadowing process. As it turns out the influence of the walls is often crucial for the dynamics of the fingers.

The structure of the paper is the following. In Sec. II, we define the model of fingered growth. In Sec. III, the derivation of a Loewner equation for the half-plane is given, following Selander [5]. The trajectories of the fingers in the half-plane are analyzed in Sec. IV. The next three sections present our results on the fingered growth in the channel and cylinder geometries, in particular, a Loewner equation for the reflecting channel is derived in Sec. V and its solutions are analyzed in Sec. VII, whereas in Sec. VI the connection between the reflecting channel and cylindrical geometry is examined. Finally, we conclude in Sec. VIII.

II. MODEL

With this introduction, let us formulate the model of fingered growth to be considered. The growth takes place at the

tips of a finite number n of infinitely thin fingers $\Gamma_i(t)$ (disjoint Jordan arcs),

$$\Gamma_i(t) \subset \mathbb{W}, \quad i = 1, \ldots, n, \tag{3}$$

where $\mathbb{W}$ is the domain in which the growth takes place and where the Laplace equation needs to be solved. The fingers extend from the boundary of $\mathbb{W}$ toward its interior in such a way that $\Gamma_i(t) \subset \Gamma_i(t')$ for $t' > t$. Additionally, on both the phase interface (along the boundary of $\mathbb{W}$) and along the fingers the condition $u(\mathbf{r},t)=0$ is imposed.

Since the finger is assumed to be infinitely thin, there is a singularity in a field gradient at its tip. Namely, at a small distance r from the tip of the ith finger, the gradient takes the form

$$\nabla u(\mathbf{r},t) = \frac{C_i(t)}{2\sqrt{r}}[\cos(\theta/2)\mathbf{e}_r + \sin(\theta/2)\mathbf{e}_\theta], \tag{4}$$

where the coefficients $C_i(t)$ depend on the lengths and shapes of all the fingers. In the above, the origin of coordinates is located at the tip of the finger and the polar axis is directed along it. Following Derrida and Hakim [21], we introduce a small circle of radius r_0 around the tip and define the finger growth rate as the integral of field gradient over the circle

$$v_i(t) = \oint \hat{n} \cdot \nabla u(\mathbf{r},t) ds = 2\sqrt{r_0} C_i(t). \tag{5}$$

Note that if the field $u(\mathbf{r},t)$ describes the concentration, then the above integral corresponds to the total particle flux through the circle. The parameter r_0 should be of the order of the finger width; its exact value does not influence the dynamics as long as we assume it to be the same for each finger. In such a case, the factor $2\sqrt{r_0}$ may be absorbed into the definition of time, and we take $v_i(t)$ equal to $C_i(t)$ [or to $C_i(t)^\eta$ in η growth].

To solve the Laplace equation we construct a time dependent map g_t as follows:

$$g_t: \ \mathbb{W} \setminus [\Gamma_1(t) \cup \cdots \cup \Gamma_n(t)] \to \mathbb{W}, \tag{6}$$

together with its inverse, f_t as follows:

$$f_t: \ \mathbb{W} \to \mathbb{W} \setminus [\Gamma_1(t) \cup \cdots \cup \Gamma_n(t)], \tag{7}$$

$$f_t \circ g_t = g_t \circ f_t = id, \quad t \geq 0, \tag{8}$$

as illustrated in Fig. 4. The function f_t can be extended to a continuous function of the boundary, which is two to one along the fingers, except of the tips where it is one to one. Thus the tips of the fingers [denoted by $\gamma_i(t)$] may be added to the domain of the function g_t with the corresponding images $a_i(t)$ as follows:

$$a_i = g_t(\gamma_i). \tag{9}$$

It may be shown (see Appendix A and also Refs. [4,5,21]) that the growth rate of a finger (5) can be expressed in terms of the map f_t as

$$v_i(t) \sim |f_t''(a_i(t))|^{-\eta/2}. \tag{10}$$

As mentioned in the Introduction, the above model of finger growth was proposed in Refs. [4,5], and independently in [6]. This model may be also looked upon as a deterministic generalization of the Meakin and Rossi [22] needle growth model—a simplified, nonbranching version of Witten and Sander's diffusion-limited aggregation (DLA) [23]. In the Meakin and Rossi model the growth is allowed to occur only in the direction away from the substrate, which results in a forest of parallel needles with a broad distribution of heights. Cates [24] obtained an average density of the aggregate in such a system in mean field approximation whereas Evertsz [25] calculated fractal dimensions of needle structures for different values of the exponent η.

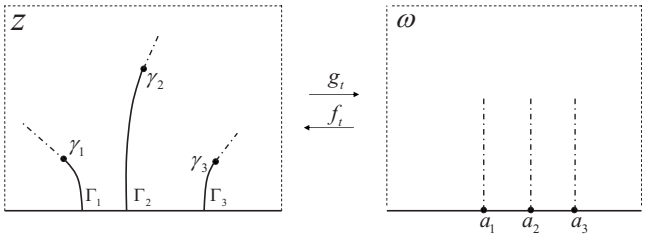

FIG. 4. An example configuration of three fingers $(\Gamma_1,\Gamma_2,\Gamma_3)$ extending from the real axis in the physical plane (z plane). The mapping g_t maps the exterior of the fingers onto the empty half-plane (ω plane). The images of the tips γ_i are located on the real line at the points $x=a_i$. The gradient lines of the Laplacian field (dot-dashed) in the z plane are mapped onto the vertical lines in the ω plane. In a given moment of time, the fingers grow along the gradient lines, the images of which pass through the points a_i.

Yet another modification of DLA was studied in the so-called "polymer-growth model" [26] where, as before, the particles were allowed to attach to the tip of the growing chain only, but the condition that the growth must occur in the direction away from the substrate was relaxed. This time, the process resulted in a set of fiberlike chains of different lengths and shapes.

The above-described, DLA-based models are stochastic in nature. On the other hand, the deterministic versions of the Meakin and Rossi needle growth model were studied by several authors [13,21,27,28], mostly by conformal mapping techniques, which were first applied to DLA-type aggregates by Shraiman and Bensimon [29], Ball [30], and Szep and Lugosi [31]. The majority of authors considered the problem in a radial geometry, with a set of straight needles growing radially from the origin, whereas in [13,28] a set of parallel needles with alternating lengths was analyzed in periodic boundary conditions. An important difference between the above-quoted needle models and the model considered here is that we do not constrain the fingers to follow the straight line; instead they can bend in the direction of the field gradient at the tip. Thus, whereas the needle models are well suited to describe a strongly anisotropic growth of rigid structures such as the sidebranching dendrites in solidification, they are less suited to describe the phenomena in which the growing structures may become deflected by the field, as is the case in the above-described combustion experiments, channel formation in the dissolving rock, or in a number of fibril-growth processes.

In the next section, we sketch the derivation of the Loewner equation for the fingered growth in the half-plane.

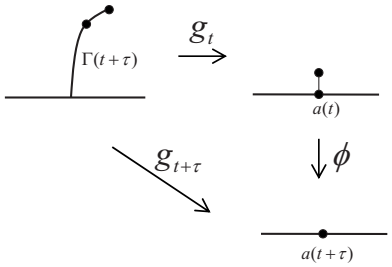

FIG. 5. Illustration of the composition of conformal maps described in the text. The mapping $g_{t+\tau}$ is obtained as the composition of g_t and the elementary slit mapping (13).

In the context of the Carleson-Makarov model, this problem was analyzed by Selander in [5]. We repeat this derivation here, because it is the simplest case which illustrates the method involved, which will be then used to tackle the channel geometry case.

III. LOEWNER EQUATION IN THE HALF-PLANE

In this section, following [5], we present the description of the fingered growth in the upper half-plane $\mathbb{C}_+ = \{z \in \mathbb{C}: \mathrm{Im}(z) > 0\}$ in terms of the conformal mappings. The solution of the Laplace equation in the empty half-plane, satisfying the boundary conditions: $u(\mathbf{r})=0$ on the real axis and $\frac{\partial u}{\partial y} \underset{y\to\infty}{\to} 1$ (constant flux at infinity), is given simply by $u(x,y)=y$. The map g_t from the exterior of the fingers to the empty half-plane will be uniquely determined by the so-called hydrodynamic normalization at infinity

$$\lim_{z\to\infty} g_t(z) - z = 0, \tag{11}$$

which ensures that the flux at infinity is unaffected by boundary movements. The map g_t is constructed by the composition (Fig. 5)

$$g_{t+\tau} = \phi \circ g_t + O(\tau^2), \tag{12}$$

where ϕ is a slit mapping

$$\phi(z) = \sqrt{[z - a(t)]^2 + h(t,\tau)^2} + a,$$
$$\phi: \ \mathbb{C}_+ \setminus \{a(t) + i[0, h(t,\tau)]\} \to \mathbb{C}_+. \tag{13}$$

It is convenient to choose $h(t,\tau)$ in the form $h(t,\tau) = \sqrt{2\tau d(t)}$, where $d(t)$ is the so-called growth factor [5]. The square root dependence of the slit length on the timestep ensures that the increment of length of the finger will be linear in τ.

Expanding Eq. (12) up to the terms linear in τ and taking the limit $\tau \to 0$ leads us to the Loewner equation for a single finger in the half-plane

$$\dot{g}_t = \lim_{\tau\to 0} \frac{\phi \circ g_t - g_t}{\tau} = \frac{d(t)}{g_t - a(t)}, \tag{14}$$

with the initial condition $g_0(z)=z$, corresponding to the empty space with no fingers. Note that the pole of Eq. (14) is located at the image of the tip, $a(t)=g_t(\gamma)$. To relate the growth factor $d(t)$ to the finger velocity let us notice that for a finite τ, the composition $\phi \circ g_t$ increases the length of the finger approximately by $\tau d(t)|f_t''(a(t))|$, thus the growth velocity is given by $v(t)=d(t)|f_t''(a(t))|$ and, using Eq. (10) we get

$$d(t) = |f_t''(a(t))|^{-\eta/2-1}. \tag{15}$$

Finally, the position of the pole a as a function of time may be found from the condition that the finger grows along the direction of the gradient near the tip. Due to the singularity at the tip, it is more convenient to work in the ω plane. Namely, the gradient lines in the physical plane (z plane) are mapped by g_t onto the vertical lines in the ω plane, as illustrated in Fig. 4. The counterimage of the veritcal line $\omega = a + is$, $s>0$ will thus define the growth direction in the z plane. In the case of a single finger, from symmetry, the gradient line in the z plane is also a vertical line—the one passing through the tip of the finger. Thus in this case the position of the pole must be constant.

$$a(t) = \mathrm{const} = a(0). \tag{16}$$

The Loewner equation can be generalized to the n-finger case by analyzing the composition of n slit mappings

$$\phi_i(z) = \sqrt{(z - a_i(t))^2 + 2\tau d_i(t)} + a_i(t), \tag{17}$$

one for each finger. The respective Loewner equation is [4,5]

$$\dot{g}_t = \sum_{i=1}^{n} \frac{d_i(t)}{g_t - a_i(t)}. \tag{18}$$

This time, however, to force the fingers to grow along gradient lines, the functions $a_i(t)$ need to change in time, since the tip images $a_i = g(\gamma_i)$ are moved by slit mappings ϕ_j with $j \neq i$. This leads to the following condition for the motion of the poles:

$$\dot{a}_i(t) = \sum_{\substack{j=1 \\ j\neq i}}^{n} \frac{d_j(t)}{a_i(t) - a_j(t)}. \tag{19}$$

The above idea of generating the growing aggregate by iterated conformal maps was applied also to the original DLA problem in a seminal paper by Hastings and Levitov [32]. In fact, the "strike" mapping proposed by them in [32] is a counterpart of the slit mapping (13) in the radial geometry. Analogous constructions for the DLA in a channel and cylindrical geometry were proposed in Ref. [33]. However, unlike the model considered here, those models were stochastic in nature, and generated noise-driven, branched, fractal structures. A deterministic version of Hastings and Levitov construction was proposed by Hastings in [6]. Although he did not use the formalism of the Loewner equation, his model is essentially analogous to that presented above.

IV. FINGERED GROWTH IN THE HALF-PLANE

Let us now look at the solutions of Eqs. (18) and (19) in a few simplest cases. As mentioned, the single-finger case is rather straightforward: the finger grows vertically along the

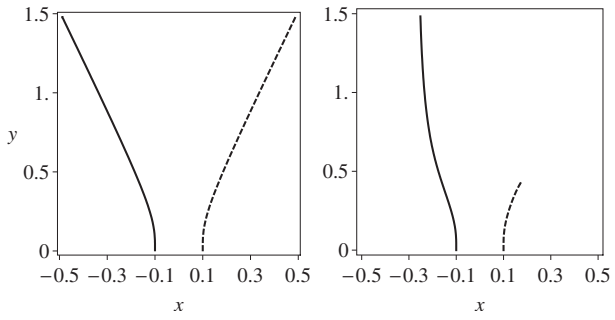

FIG. 6. Two fingers growing in the half-plane for $\eta=-2$ (left panel) and $\eta=4$ (right panel). The initial positions of the fingers are $a_1(0)=-a_2(0)=0.1$.

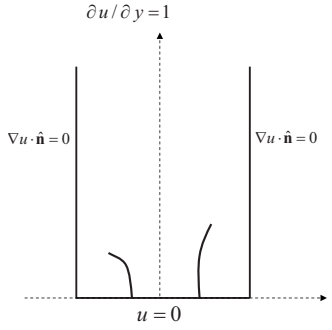

FIG. 7. The geometry of the channel together with the boundary conditions.

line $x=a$. A more interesting case is that of two fingers. Here the results depend in a significant way on the value of the exponent η used. A related problem in a slightly different geometry [growth in $\mathbb{W}\equiv\mathbb{C}\backslash\mathbb{R}_+$] was considered by Carleson and Makarov in [4]. Although their results are not directly applicable here, it is relatively straightforward to repeat their derivations for the growth in the half-plane. Namely, it turns out that there are three regimes in the behavior of the fingers, depending on the value of the exponent η. For $-\infty<\eta<\eta_c\approx 0.43$, the two fingers, irrespectively of their initial positions, grow symmetrically, as illustrated in Fig. 6. Next, for $\eta_c<\eta<\eta_c'=2/3$, the symmetric solution becomes unstable; one of the fingers starts to grow faster and screens the other. However, the screening is only partial and the ratio of finger velocities v_1/v_2 goes to a positive constant (different from 1) when $t\to\infty$. Finally, for $\eta>\eta_c'$ there is a stronger screening and the ratio of the velocity of the slower finger to that of the faster one goes to zero asymptotically.

The shape of the fingers in the first regime may be obtained analytically. To this end, it is most convenient to consider the case of $\eta=-2$ which, according to Eq. (15), corresponds to the evolution with constant growth factors $d_1=d_2\equiv d_0$. For further analysis, we choose the coordinates in such a way that $a_1(0)=-a_2(0)=a_0$. Equation (19) may be then readily integrated to yield

$$a_{1,2}(t)=\pm\sqrt{a_0^2+d_0t}. \tag{20}$$

Inserting the above into the Loewner equation (18), we can find g_t and then obtain the positions of the tips $\gamma_i(t)$ as a function of time. They are given implicitly by

$$\pm 16(a_0^2+d_0t)^{5/2}=\gamma_{1,2}(t)[\gamma_{1,2}(t)^2-5a_0^2]^2, \tag{21}$$

where we take only the roots which lie in the upper half-plane and satisfty the initial condition $\gamma_i(0)=a_i(0)$. An example trajectory with $a_0=0.1$ is shown in Fig. 6. We see that the fingers repel each other, which is due to the term $1/(a_j-a_i)$ in the evolution equation of the poles (19). Asymptotically, as $t\to\infty$, the relation (21) takes the form

$$\pm 16(d_0t)^{5/2}=(\gamma_i(t))^5, \tag{22}$$

from which it may be concluded that the fingers tend to the straight lines $\arg(z)=\frac{2\pi}{5}$ and $\arg(z)=\frac{3\pi}{5}$ with the angle $\pi/5$ between them. Although the above result was obtained for the $\eta=-2$ case, as mentioned above, such a symmetric solution remains stable up to η_c. Thus, in this range of η the fingers follow the same trajectories as in Fig. 6, but with different velocities than those in the $d=$const case. In fact, whenever the fingers grow symmetrically, with equal growth factors, $d_1(t)=d_2(t)$, one may always rescale the time coordinate by defining $t'=\int_0^t d_1(t'')dt''$ and thus reduce the problem to the constant growth factor ($d_1=d_2=1$) case.

The right panel of Fig. 6 shows the shape of the finger in the strongly unstable case, $\eta=4$. In this case the solution was obtained numerically, as described in Appendix B. As is observed, initially the tips follow the same trajectory as in the stable case, but then due to the numerical noise in the computations, the instability sets in, one of the fingers outgrows the other and then continues along the vertical direction. The other finger slows down and the ratio of its velocity to that of the winning finger goes to zero.

The fact that there is a range of positive values of η for which the symmetric solution is stable seems surprising at first sight. However, in the unbounded domain the fingers have the possibility to escape from each other to the regions where the influence of another finger is smaller. Such a behavior may hardly be observed in a bounded system because of the wall effect which makes it impossible for the fingers to escape from each other. In the next section, we show how to take into account the presence of the sidewalls in the system and how their presence affects the dynamics of the fingers.

V. LOEWNER EQUATION IN THE CHANNEL GEOMETRY

In this section we consider the growth of the fingers in the channel geometry, i.e., in the domain

$$\mathbb{P}=\{z=x+iy\in\mathbb{C}:\ y>0,\quad x\in\,]-1,1[\}, \tag{23}$$

with the boundary conditions $u=0$ at a bottom wall $[-1,1]$ and along the fingers, and $\frac{\partial u}{\partial x}=0$ on the sides (which corresponds to reflecting boundary conditions at the impenetrable sidewalls) and $\frac{\partial u}{\partial y}=1$ at infinity (see Fig. 7). For an empty channel with the above boundary conditions, the solution of the Laplace equation is again given by $u(x,y)=y$, in full analogy to the half-plane case. Our goal is to construct the mapping g_t,

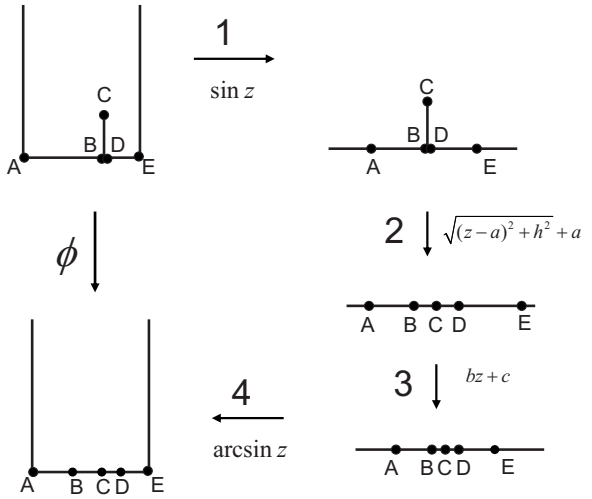

FIG. 8. Schematic picture of the mappings used in construction of elementary slit mapping ϕ in the channel geometry.

$$g_t:\ \mathbb{P}\setminus[\Gamma_1(t)\cup\cdots\cup\Gamma_n(t)]\to\mathbb{P}, \tag{24}$$

together with its inverse f_t. The boundary condition at the bottom wall is different from that at the sides, thus the points -1 and 1 must remain fixed under the mapping f_t, or, in terms of g_t,

$$\lim_{z\to-1} g_t(z)+1=\lim_{z\to1} g_t(z)-1=0. \tag{25}$$

Additionally, we require that g_t keeps the point at infinity fixed, i.e.,

$$\mathrm{Im}(g_t(z))\to\infty \quad \text{for} \quad \mathrm{Im}(z)\to\infty. \tag{26}$$

Those conditions define the conformal map g_t uniquely.

First let us consider the case of a single finger. The derivation of the Loewner equation in this case will be analogous to that presented above for the half-plane. However, the slit mapping is now different. The idea of construction of the mapping is shown in Fig. 8. As before, we begin with a short slit of length $h=\sqrt{2\tau d}$. The first function "1" transforms $\mathbb{P}$ into the half-plane keeping points $A=-1$, $E=1$ fixed and is given by $\sin(\frac{\pi}{2}z)$. When the slit length is small, $h\ll1$, its length after the transformation 1 can be calculated from the Taylor expansion up to linear terms in τ,

$$\sin\left(\frac{\pi}{2}(a+i\sqrt{2\tau d})\right)\approx\left(1+\frac{\pi^2}{4}\tau d\right)\sin\left(\frac{\pi}{2}a\right)+\frac{i\pi}{2}\sqrt{2\tau d}\cos\left(\frac{\pi}{2}a\right)+\cdots. \tag{27}$$

Denoting the new length of the slit by $\sqrt{2\tau d'}$ we get

$$d'=d\frac{\pi^2}{4}\cos^2\left(\frac{\pi}{2}a\right)+O(\tau^2). \tag{28}$$

Function "2" is the slit mapping in the half-plane given by Eq. (13). The composition of 1 and 2 reads then

$$\varphi(z)=\sqrt{\left[\sin\left(\frac{\pi}{2}z\right)-\beta\sin\left(\frac{\pi}{2}a\right)\right]^2+2\tau d'}, \tag{29}$$

where $\beta=(1+\frac{\pi^2}{4}\tau d)$. The above slit mapping moves the points A and E. To shift them back to -1 and 1, we use an additional map, "3," which is a linear function with real parameters. The map "4" is just the inverse of 1, i.e., $\frac{2}{\pi}\arcsin(z)$. The final form of ϕ is thus given by

$$\phi(z)=\frac{2}{\pi}\arcsin\left[\frac{2\varphi(z)-[\varphi(1)+\varphi(-1)]}{\varphi(1)-\varphi(-1)}\right]. \tag{30}$$

Keeping only the terms linear in τ,

$$\phi(z)=z+\tau d\frac{\pi}{2}\frac{\cos(\frac{\pi}{2}z)}{\sin(\frac{\pi}{2}z)-\sin(\frac{\pi}{2}a)}+O(\tau^2), \tag{31}$$

we obtain the Loewner equation of the form

$$\dot{g}_t=d(t)\frac{\pi}{2}\frac{\cos(\frac{\pi}{2}g_t)}{\sin(\frac{\pi}{2}g_t)-\sin(\frac{\pi}{2}a(t))}. \tag{32}$$

Note that due to the presence of the sidewalls the slit mapping is no longer symmetric, in the sense that the images of the points B and D at the base of the finger are asymmetric with respect to the image of C (cf. Fig. 8). This means that, in contrast to the half-plane case, the pole $a=g_t(\gamma)$ will be shifted by the mapping. This shift may be obtained from the Loewner equation in the limit $g_t(z)\to a$. However, the equation is singular at that point, thus we take the symmetric limit from both sides toward a singularity as follows:

$$\dot{a}(t)=\lim_{\epsilon\to0}\frac{W(a-\epsilon)+W(a+\epsilon)}{2}, \tag{33}$$

where $W(g)=d\frac{\pi}{2}\cos(\frac{\pi}{2}g)/[\sin(\frac{\pi}{2}g)-\sin(\frac{\pi}{2}a)]$. Explicit evaluation of the limit yields

$$\dot{a}(t)=-\frac{\pi}{4}d(t)\tan\left(\frac{\pi}{2}a(t)\right). \tag{34}$$

The equation for the n-finger case may be obtained, as before, by the composition of n-slit mappings, one for each finger, which leads to

$$\dot{g}_t=\frac{\pi}{2}\sum_{i=1}^{n} d_i\frac{\cos(\frac{\pi}{2}g_t)}{\sin(\frac{\pi}{2}g_t)-\sin(\frac{\pi}{2}a_i)}. \tag{35}$$

Finally, to derive the condition for the motion of the poles in the n-finger case, we need to add self terms of the form (34) and the interaction terms, which may be obtained from Eq. (35) by taking $g_t=a_j$ with $i\neq j$. This leads to

$$\dot{a}_j=-\frac{\pi}{4}d_j\tan\left(\frac{\pi}{2}a_j\right)+\frac{\pi}{2}\sum_{\substack{i=1\\ i\neq j}}^{n} d_i\frac{\cos(\frac{\pi}{2}a_j)}{\sin(\frac{\pi}{2}a_j)-\sin(\frac{\pi}{2}a_i)}. \tag{36}$$

The presence of the self term, Eq. (34), attracts the pole to $a=0$, which is a stable fixed point of Eq. (34) and causes the finger to bend in the direction of the centerline of the

channel. It is most clearly seen in the single-finger case. For the constant growth factor $d(t)=d_0$ (which corresponds to $\eta=-2$), Eq. (34) may be solved explicitly to yield

$$\sin\left(\frac{\pi}{2}a_t\right) = e^{-(\pi^2 d_0/8)t}\sin\left(\frac{\pi}{2}a_0\right). \tag{37}$$

Thus, $\sin(\frac{\pi}{2}a_t)$ goes to zero exponentially. A corresponding trajectory of the finger may be expressed implicitly through elliptic integrals and is shown in Fig. 9. As it is observed, the finger starts at $z=a(0)$, initially grows perpendicularly to the bottom wall, but very soon the influence of the walls becomes important and the finger is attracted to the symmetric position in the center of the channel. As explained previously, for other values of η the shape of the finger is the same as that presented above, only its velocity changes.

Naturally, if the initial position of the finger is already in the middle of the channel, $a(0)=0$, it would simply continue growing along the centerline. In that case the map f_t is given by

$$f_t(z) = \frac{2}{\pi}\arcsin\left[\sqrt{\sin^2\left(\frac{\pi}{2}z\right)\cosh^2\left(\frac{\pi}{2}H(t)\right) - \sinh^2\left(\frac{\pi}{2}H(t)\right)}\right], \tag{38}$$

where $H(t)$ is the height of the finger at a given moment of time. In particular,

$$|f_t''(0)| = \frac{\pi}{2}\coth\left(\frac{\pi}{2}H(t)\right), \tag{39}$$

which gives the velocity of the tip as

$$v(H) = \left[\frac{\pi}{2}\coth\left(\frac{\pi}{2}H\right)\right]^{-\eta/2}. \tag{40}$$

The asymptotic velocity of the finger is thus

$$v_{as} = \lim_{H\to\infty} v(H) = \left(\frac{\pi}{2}\right)^{-\eta/2}, \tag{41}$$

and the asymptotic growth factor is [cf. Eq. (15)]

$$d_{as} = \left(\frac{\pi}{2}\right)^{-\eta/2-1}. \tag{42}$$

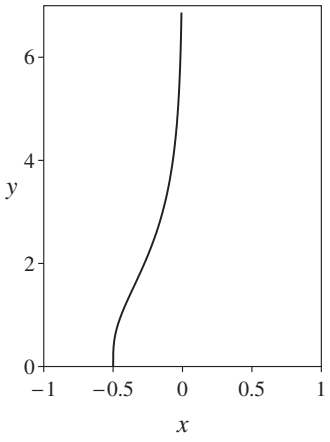

FIG. 9. The growth of a single finger in the channel with $a(0)=-0.5$.

It is instructive to compare this result with that for a single finger growing in the half-plane. In the latter case $f_t(z)=\sqrt{z^2-H^2(t)}$ and the velocity obeys

$$v(H) = H^{\eta/2}, \tag{43}$$

hence, for $\eta>0$, it is growing indefinitely as the finger increases its height. This is to be expected since in the unbounded case, as the finger is getting further away from the absorbing wall, it intercepts an increasingly larger flux. Contrastingly, in the case of the channel, the total flux through its cross section is finite, and the growth rate of the finger stabilizes as soon as its height becomes large in comparison to the channel width. Note that the result (43) for the half-plane may also be recovered by expanding the formula (40) in $H \ll 1$, since $\frac{\pi}{2}\coth(\frac{\pi}{2}H)=H^{-1}+\cdots$. Thus, at the beginning of the evolution, the finger behaves as if it were in an unbounded domain; soon, however, the presence of the sidewalls becomes a determining factor in its dynamics.

VI. GROWTH IN THE CYLINDER GEOMETRY

The above formalism may also be used to find the evolution of the fingers in a channel with periodic boundary conditions as follows:

$$u(x+2,y) = u(x,y), \tag{44}$$

topologically equivalent to the surface of a semi-infinite cylinder. Namely, consider a single finger growing in the periodic channel with the initial position of the pole $a(0)=a_0$. Translating the origin to a_0 we obtain a single finger growing vertically in the middle of the channel on the sidewalls of which both periodic and reflecting boundary conditions are satisfied simultaneously. The growth of this finger is described by the Loewner equation (32) with $a=0$. Transforming back to the original coordinates one obtains

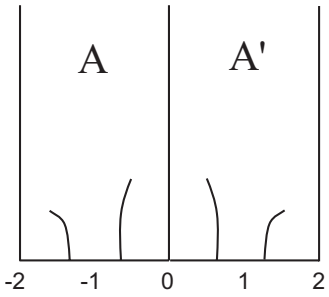

FIG. 10. The channel A and its mirror reflection A'.

$$\dot{g}_t = d\frac{\pi}{2}\cot\left(\frac{\pi}{2}(g_t - a)\right), \tag{45}$$

which is the Loewner equation for a single finger in the cylinder. This equation has already been derived [4,19] in the context of growth processes in radial geometry (which may then be mapped onto cylindrical by the map of the form $z \to \ln z$). However, yet another, and perhaps easier, derivation of Eq. (45) may be given, starting form the Loewner equation for the half-plane (14) and summing over the pairs of periodic images of the pole: $a_j = a \pm 2j$, $j = 1, 2, \ldots$. This gives

$$\dot{g}_t = \frac{1}{g_t - a} + \sum_{j=1}^{\infty}\left(\frac{d}{g_t - (a+2j)} + \frac{d}{g_t - (a-2j)}\right)$$
$$= d\frac{\pi}{2}\cot\left(\frac{\pi}{2}(g_t - a)\right). \tag{46}$$

The generalization of the Loewner equation to the n-finger case proceeds along the same lines as before and yields

$$\dot{g}_t = \sum_i d_i\frac{\pi}{2}\cot\left(\frac{\pi}{2}(g_t - a_i)\right), \tag{47}$$

whereas the equation of motion of the poles reads

$$\dot{a}_j = \sum_{i\neq j} d_i\frac{\pi}{2}\cot\left(\frac{\pi}{2}(a_j - a_i)\right). \tag{48}$$

This time the self-term (34) is absent since the situation is again symmetric and the single-finger slit mapping does not affect the position of the corresponding pole.

Above, we derived the dynamics of the fingers in the cylinder based on the Loewner equation for the channel. It is also instructive to follow the opposite direction and derive the Loewner equation for the channel starting with Eq. (45). As it turns out, such an approach provides us with the clear interpretation of the self-term (34).

To start with, consider n fingers growing in a channel with reflecting boundaries (designated by A in Fig. 10). Next, let us reflect the system with respect to one of its sidewalls and denote the image by A'. Thus, there are now $2n$ fingers: the original ones $\{1, \ldots, n\}$ in A and their images $\{n+1, \ldots, 2n\}$ in A'. Due to the reflection symmetry

$$a_i = -a_{n+i}, \quad d_i = d_{n+i}, \quad i \in \{1, \ldots, n\}, \tag{49}$$

with coordinates chosen so that $x=0$ corresponds to the joint wall of the two channels, as in Fig. 10. Finally, we look for the solution of the Laplace equation in the joint system (AA') in periodic boundary conditions. Due to the symmetry, such a solution will automatically satisfy the reflecting boundary conditions in A.

To be more formal, the Loewner equation in the AA' channel will be given by

$$\dot{g}_t = \frac{\pi}{4}\sum_{i=1}^{2n} d_i \cot\left(\frac{\pi}{4}(g_t - a_i)\right), \tag{50}$$

which is equivalent to Eq. (47) additionally rescaled by a factor of 2 to account for the fact that the width of AA' is twice the width of A. Taking into account Eq. (49), we get

$$\dot{g}_t = \frac{\pi}{4}\sum_{i=1}^{n} d_i\left[\cot\left(\frac{\pi}{4}(g_t - a_i)\right) + \cot\left(\frac{\pi}{4}(g_t + a_i)\right)\right], \tag{51}$$

which, by straightforward trigonometry, leads to

$$\dot{g}_t = -\sum_{i=1}^{n} d_i\frac{\pi}{2}\frac{\sin(\frac{\pi}{2}g_t)}{\cos(\frac{\pi}{2}g_t) - \cos(\frac{\pi}{2}a_i)}. \tag{52}$$

Finally, we move the origin of coordinates to the center of A by

$$z' = z + 1, \tag{53}$$

which leads us to the Loewner equation for the channel (35). The equation of motion of the poles may be transformed along the similar lines as follows:

$$\dot{a}_j = d_j\frac{\pi}{4}\cot\left(\frac{\pi}{4}(a_j - a_{n+j})\right) + \sum_{\substack{i=1 \\ i\neq j,n+j}}^{2n} d_i\frac{\pi}{4}\cot\left(\frac{\pi}{4}(a_j - a_i)\right). \tag{54}$$

The first term describes the interaction between the pole a_j and its image a_{n+j} and, using Eqs. (49) and reverting to the original coordinates, may be transformed to $-\frac{\pi}{4}d_j\tan(\frac{\pi}{2}a_j)$, which is exactly the self-term (34) derived before. The terms in the remaining sum, using Eq. (49) and reverting to the original coordinates, may be written in the form $d_i\frac{\pi}{2}\cos(\frac{\pi}{2}a_j)/[\sin(\frac{\pi}{2}a_j) - \sin(\frac{\pi}{2}a_i)]$, in agreement with Eq. (36).

The above derivation shows, in particular, that the stable, symmetric solution of two-finger growth in the cylinder may be reduced to the previously considered problem of a single-finger growth in the channel. Indeed, Fig. 11 shows two-finger solution in the cylinder the initial conditions $a_{1,2}(0) = \pm 0.25$ (if the fingers are initially not symmetric with respect to zero they can be rendered so by an appropriate change of variables). It is observed that the right-hand side finger has the same shape as that in Fig. 9, whereas the left-hand side one is its mirror reflection.

Figure 11 illustrates an important property of stable solutions of n fingers growing in the cylinder. Namely, irrespectively of initial positions, the fingers end up in the symmetric configuration, with equal distances between each other. This is a direct consequence of the repulsion between the poles, as

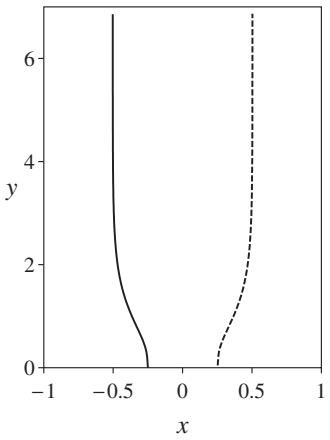

FIG. 11. Two fingers growing in the cylinder with $a_{1,2}(0) = \pm 0.25$ and $\eta=-2$ (stable symmetric solution).

described by Eq. (48). Indeed, it is seen that the uniform arrangement of the poles constitutes a fixed point of Eq. (48).

Because of the relation between the geometry of a reflecting channel and that of a cylinder, the above statement may also serve to prove that, in the stable case, both the fingers and the poles in the channel end up at the positions $x_i=(2i-1)/n-1$, where n is the number of fingers and $i=1,\ldots,n$.

VII. COMPETITION BETWEEN FINGERS IN THE CHANNEL

In this section we look more closely at the instabilities in the growth of two fingers both in the channel and in the cylinder, paying particular attention to the screening process and competition between the fingers. The results presented in this section, unlike those presented in Figs. 9 and 11, are obtained by numerical calculation (as described in Appendix B).

As mentioned in Sec. IV, in the case where fingers grow in the half-plane, there exists a critical value of the exponent (η_c) below which the symmetric solution is stable and another threshold value, η_c', such that for $\eta_c<\eta<\eta_c'$, there exists an asymmetric solution of the growth of two fingers with the velocity ratio of the slower finger to that of the faster one, $\frac{v_1}{v_2}$, asymptotically approaching the value different both from 0 and 1. Here we argue that for the channel, either reflecting or periodic, $\eta_c=\eta_c'=0$, i.e., the growth is unstable for any positive η, with $\frac{v_1}{v_2}\to 0$. Such a fundamental difference between the two systems is connected with the geometries involved [34]. Consider the late stages of the screening process, with a shorter finger (of length l_1) situated in a deep fjord between two longer fingers (or a longer finger and its periodic image) of length l_2. The value of the Laplacian field u near the tip of the short finger then obeys

$$u \sim e^{-\pi(l_2-l_1)/a}, \quad l_2 \gg l_1, \tag{55}$$

where a is the width of the fjord. As mentioned, in the half-plane case the fingers asymptotically tend to straight lines growing radially from the origin, thus in that case the fjords will have a wedgelike shape (cf. Fig. 12). For such a fjord with an internal angle θ one finds

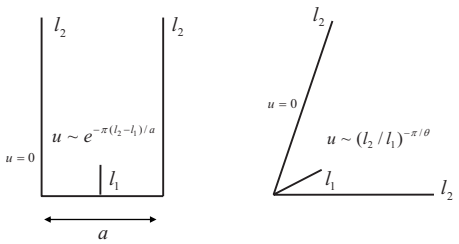

FIG. 12. The scaling of a Laplacian field u in rectangular and wedgelike fjords.

$$u \sim \left(\frac{l_2}{l_1}\right)^{-\pi/\theta}, \quad l_2 \gg l_1. \tag{56}$$

Thus the screening in the channel geometry is exponential, whereas in the half-plane it follows a power law. Consequently, in the latter case, we can choose the values of η and θ in such a way that would guarantee that the ratio of the velocities of the fingers is equal to their length ratio

$$\frac{l_1}{l_2} = \frac{v_1}{v_2}, \tag{57}$$

which corresponds to the (asymmetric) solution of the fingers dynamics which is stationary in the sense that the ratio l_1/l_2 remains constant.

Contrastingly, for the exponential screening, irrespectively of the values of a and η (as long as it is positive) the velocity of the shorter finger always decreases to zero, thus also $l_1/l_2\to 0$: the screening is complete.

Figure 13 presents an example of such a situation. Here, two fingers are evolving in the channel with either reflecting or periodic walls at $\eta=1$. At the beginning, the fingers repel each other and behave very similarly to the stable, symmetric solution with $\eta<0$ (cf. Fig. 14). However, as soon as their height becomes comparable to the width of the channel, the instability sets in and initially small differences in the height of the fingers are rapidly amplified. As observed in Fig. 13,

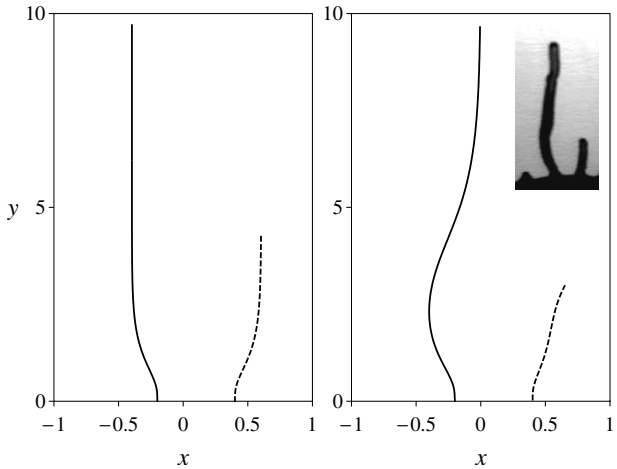

FIG. 13. Two fingers growing in the cylinder (left panel) and in the reflecting channel (right panel) for $\eta=1$. The initial positions of the fingers are $a_1(0)=-0.2$ and $a_2(0)=0.4$. Inset: the interaction of two fingers in the combustion experiments of Zik and Moses [3].

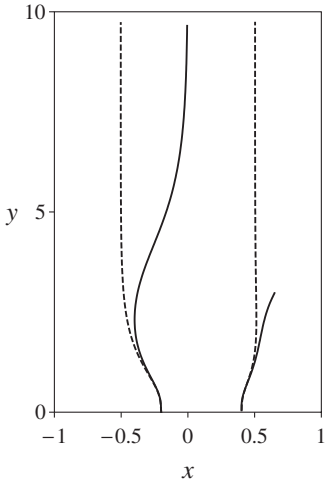

FIG. 14. Two fingers growing in the reflecting channel at $\eta=1$ (solid line) and $\eta=-2$ (dashed). The initial positions of the fingers are the same as those in Fig. 13.

in the reflecting channel the longer (winning) finger is attracted to the centerline (as it is the case for the single-finger solution), whereas in the cylinder it continues to grow vertically.

The analysis of Fig. 13 together with the corresponding dependencies of the growth velocity on time presented in Fig. 15 shows distinctly three different stages of finger growth. In the initial stage, the fingers repel each other, their velocities increase quickly but remain equal to each other; the competition between the fingers is not yet present. Then, as the distance between the fingers approaches 1, their velocities stabilize at around $v\approx 0.6$. In fact, the velocities of the fingers in this stage are close to the asymptotic velocity of a single finger in the channel of half the width of the original one, i.e., analogously to Eq. (41),

$$v=\frac{1}{2}\left(\frac{\pi}{4}\right)^{-1/2}\approx 0.56, \tag{58}$$

which agrees with the value 0.6 quoted above. As seen in Fig. 14 the unstable $\eta=1$ solution diverges from the stable one ($\eta=-2$) when the height of the finger reaches approximately 1–2 units, i.e., becomes comparable with the channel width. This is where the final stage of the evolution begins, with a sharp decrease of the velocity of the losing finger and the corresponding increase of the velocity of the winning one up to the asymptotic value $v_{as}=(\pi/2)^{-1/2}\approx 0.798$. [cf. Eq. (41)]. Note that in the case of the cylinder it is impossible to

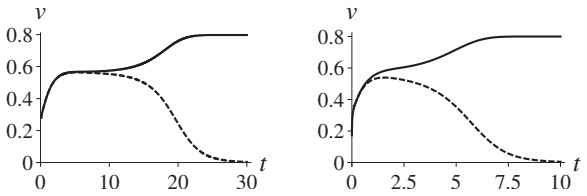

FIG. 15. The velocities of the fingers as a function of time in the cylinder (left) and in the channel (right), corresponding to the fingers of Fig. 13.

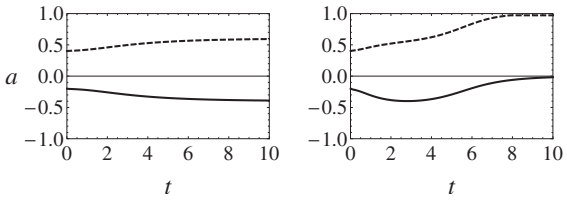

FIG. 16. The positions of the poles as a function of time, in the cylinder (left) and in the channel (right), corresponding to the fingers of Fig. 13.

predict beforehand which finger is expected to win the competition—the initial situation is fully symmetric and, in principle, the system could remain in the unstable symmetric state were it not for the numerical noise (no other sources of noise are present). Contrastingly, in the reflecting channel, the finger which starts closer to the centerline is destined to win, since, during its evolution it moves through regions of higher field gradient.

Further insight into the competition process may be gained by analyzing the evolution of the poles, as presented in Fig. 16. It is seen that in the channel the pole of the winning finger is attracted toward the center, whereas the pole of the suppressed finger moves to the side of the channel. This can be explained by replacing in Eq. (36) the growth factors d_i by their asymptotic values: $d_1=d_{as}$ [cf. Eq. (42)] for the winning finger and $d_2=0$ for the losing one. This leads to

$$\dot{a}_1=-\frac{\pi}{4}d_{as}\tan\left(\frac{\pi}{2}a_1\right),$$

$$\dot{a}_2=\frac{\pi}{2}d_{as}\frac{\cos(\frac{\pi}{2}a_2)}{\sin(\frac{\pi}{2}a_2)-\sin(\frac{\pi}{2}a_1)}. \tag{59}$$

The asymptotic fixed point of the first equation is $a_1=0$, in full analogy to the single-finger solution in the channel. It is then inserted into the second equation to yield

$$\dot{a}_2=\frac{\pi}{2}d_{as}\cot\left(\frac{\pi}{2}a_2\right), \tag{60}$$

with the asymptotic fixed points at $a_2=\pm 1$.

In the inset of Fig. 13, we reproduce a two-finger pattern from the combustion experiments by Zik and Moses. The resemblance is remarkable. Nevertheless, we do not claim that such a simple model can accurately reproduce the complex dynamics of combustion in the Hele-Shaw cell, we can only conclude that the fingers in those experiments indeed seem to follow the gradient lines of the Laplacian field (which in this case represents the concentration of oxygen at a given point), and that there is a screening mechanism leading to the competition between the fingers. This does not mean necessarily that the velocity of the finger must be connected with the field gradient analogously to Eq. (2). In fact, many of the results of the above presented model are independent of the actual relation between the velocity v and the field u. In particular, the shape of the single-finger solution and the symmetric two-finger solution are independent of the

$v(u)$ relation, which affects in this case only the overall growth rate, not the finger shape. The same does not hold for asymmetric solutions, but even in that case some of the qualitative features of the dynamics, which give the winning finger in Fig. 13 its characteristic shape remain universal: at the beginning the fingers are attracted to the symmetric solutions, then the instability sets in and finally, the winning finger is attracted to the centerline.

VIII. SUMMARY

In this paper we have studied a simple model of Laplacian growth, in which the fingerlike protrusions grow only at their tips. In contrast to the needle-growth models, considered previously in the literature [13,21,27,28], here the fingers are allowed to bend along the gradient of the Laplacian field. The method of iterated conformal maps was applied to solve the growth problem in the geometry of the channel with two reflecting walls. We derived the Loewner equation for such a geometry and analyzed its analytical and numerical solutions in one- and two-finger cases. It was shown that the finger growth in the channel is qualitatively different from that in the unbounded space. In particular, the competition between the fingers is much stronger in the case of the channel and, for any positive value of the exponent η, the only stable asymptotic situation is that of a single finger, which had outgrown the others and continues to grow with a constant velocity along the centerline of the channel, whereas the other fingers stop growing completely.

ACKNOWLEDGMENTS

Valuable discussions with Adam Szereszewski are gratefully acknowledged. The photos of the combustion experiments are courtesy of Professor Elisha Moses from the Weizmann Institute of Science. This project has been supported by the Polish Ministry of Science and Higher Education (Grant No. N202023 32/0702).

APPENDIX A: EXPRESSION FOR FINGER VELOCITY IN TERMS OF THE MAP f_t

In this appendix a sketch of the proof of Eq. (10) is presented. This equation relates the finger velocity to $f_t''(a)$—the second derivative of f_t mapping calculated at the image of the tip. To prove Eq. (10), it is convenient to introduce the analytic complex potential Θ, such that $u=\mathrm{Im}\,\Theta$. Then, in the ω plane, corresponding to the empty half-plane (or channel), the solution satisfying the boundary condition $u(\omega)=0$ on the real axis is $\Theta(\omega)=\omega$. The corresponding complex potential in the z plane is then simply $\Theta(g_t(z))=g_t(z)$. The derivative of the complex potential is directly connected to the gradient of u, in particular,

$$\left|\frac{dg_t}{dz}\right| = |\nabla u|. \tag{A1}$$

Ignoring for the moment the singularity at the tip ($z=\gamma$), let us try to calculate the derivative of the g at that point

$$\left.\frac{dg_t}{dz}\right|_{z=\gamma} = \lim_{\delta\to 0}\frac{g_t(\gamma+\delta)-g_t(\gamma)}{\delta} = \lim_{\delta\to 0}\frac{a+\epsilon(\delta)-a}{\delta} = \lim_{\delta\to 0}\frac{\epsilon(\delta)}{\delta}, \tag{A2}$$

where $a+\epsilon$ is the image of the point $\gamma+\delta$ under g_t.

On the other hand,

$$\delta = f_t(a+\epsilon)-f_t(a) = f_t'(a)\epsilon + \frac{1}{2}f_t''(a)\epsilon^2 + \cdots. \tag{A3}$$

The first term on the right-hand side vanishes, since f has a local maximum at a, corresponding to the tip of the finger, thus $\epsilon=[2\delta/f_t''(a)]^{1/2}$ and the expression for the gradient takes form,

$$\left.\frac{dg_t}{dz}\right|_{z=\gamma} = \lim_{\delta\to 0}[\delta f_t''(a)/2]^{-1/2}, \tag{A4}$$

with the singularity at $\delta=0$, as expected. Using the regularization described in Sec. II to remove the factor $\delta^{-1/2}$ we get finally

$$|v| \sim |f_t''(a)|^{-\eta/2}. \tag{A5}$$

APPENDIX B: NUMERICAL METHOD

In this appendix, we describe briefly the numerical method used to follow the evolution of the fingers. Instead of integrating the Loewner equation, as it is done, e.g., in Ref. [35], we obtain the mapping g_t by direct iteration of the elementary slit mappings [which are of the form (17) for the half-plane and (30) for the channel geometry]. Since there are n fingers, each timestep involves the composition of n-slit mappings ϕ_i, each characterized by a corresponding position of the pole a_i, and the growth factor d_i. In the case of the cylinder, the corresponding slit mapping may also be obtained from Eq. (30) by a procedure described in Sec. VI: for a finger with the pole at a_i, first the system of coordinates is translated by $z\to z-a_i$, then the slit mapping (30) is applied [the corresponding pole is now located at the origin, thus $a=0$ is to be put in Eq. (29)] and the result is transformed back to the original coordinate system: $z\to z+a_i$. The calculations are somewhat complicated by the dependence of the growth factors d_i on the $f_t(a_t)$, as given by Eq. (15). However, as before, this map may also be obtained by the composition of elementary mappings $\tilde{\phi}$, which are the inverses of slit mappings ϕ, i.e., $\tilde{\phi}(\phi(z))=z$. The second derivative of f_t may then be calculated either analytically, by differentiating the composition of all the slit mappings which make up f_t, or by a direct numerical differentiation. The latter method is faster, whereas the former is more accurate, which becomes important at the late stages of finger competition, where the growth factor of the losing finger becomes very small.

[1] T. Vicsek, *Fractal Growth Phenomena* (World Scientific, Singapore, 1989).
[2] P. Meakin, *Fractals, Scaling and Growth Far From Equilibrium* (Cambridge University Press, Cambridge, England, 1998).
[3] O. Zik and E. Moses, Phys. Rev. E **60**, 518 (1999).
[4] L. Carleson and N. Makarov, J. Anal. Math. **87**, 103 (2002).
[5] G. Selander, Ph.D. thesis, Royal Institute of Technology, Stockholm, Sweden, 1999 (unpublished).
[6] M. B. Hastings, Phys. Rev. E **64**, 046104 (2001).
[7] A. Kuhn and F. Argoul, Phys. Rev. E **49**, 4298 (1994).
[8] P. Szymczak and A. J. C. Ladd, Geophys. Res. Lett. **33**, L05401 (2006).
[9] Y. Couder, F. Argoul, A. Arnéodo, J. Maurer, and M. Rabaud, Phys. Rev. A **42**, 3499 (1990); Y. Couder, J. Maurer, R. González-Cinca, and A. Hernández-Machado, Phys. Rev. E **71**, 031602 (2005).
[10] M. Dogterom and S. Leibler, Europhys. Lett. **24**, 245 (1993); Phys. Rev. Lett. **70**, 1347 (1993).
[11] O. Zik, Z. Olami, and E. Moses, Phys. Rev. Lett. **81**, 3868 (1998).
[12] C. Lu and Y. C. Yortsos, Phys. Rev. E **72**, 036201 (2005).
[13] P. M. J. Krug, K. Kessner, and F. Family, Europhys. Lett. **24**, 527 (1993); Y. Huang, G. Ouillon, H. Saleur, and D. Sornette, Phys. Rev. E **55**, 6433 (1997).
[14] S. A. Curtis and J. V. Maher, Phys. Rev. Lett. **63**, 2729 (1989).
[15] J. A. Warren and J. S. Langer, Phys. Rev. E **47**, 2702 (1993); M. Q. Lopez-Salvans, J. Sasademunt, G. Iori, and F. Sangues, Physica D **164**, 127 (2002).
[16] K. Löwner, Math. Ann. **89**, 103 (1923).
[17] P. L. Duren, *Univalent Functions* (Springer, New York, 1983); M. Rosenblum and J. Rovnyak, *Topics in Hardy Classes and Univalent Functions* (Birkhäuser, New York, 1994).
[18] I. A. Gruzberg and L. P. Kadanoff, J. Stat. Phys. **114**, 1183 (2004).
[19] M. Bauer and D. Bernard, Phys. Rep. **432**, 115 (2006).
[20] W. Kager and B. Nienhuis, J. Stat. Phys. **115**, 1149 (2004); G. F. Lawler, *Conformally Invariant Processes in the Plane* (American Mathematical Society, Providence, 2005); M. Bauer and D. Bernard, Commun. Math. Phys. **239**, 493 (2003).
[21] B. Derrida and V. Hakim, Phys. Rev. A **45**, 8759 (1992).
[22] G. Rossi, Phys. Rev. A **34**, 3543 (1986); P. Meakin, *ibid.* **33**, 1984 (1986).
[23] T. A. Witten and L. M. Sander, Phys. Rev. Lett. **47**, 1400 (1981).
[24] M. E. Cates, Phys. Rev. A **34**, 5007 (1986).
[25] C. Evertsz, Phys. Rev. A **41**, 1830 (1990).
[26] R. M. Bradley and D. Kung, Phys. Rev. A **34**, 723 (1986); J. M. Debierre and L. Turban, J. Phys. A **19**, L131 (1986); P. Meakin, Phys. Rev. A **37**, 2644 (1988).
[27] M. A. Peterson, Phys. Rev. Lett. **62**, 284 (1989); Phys. Rev. E **57**, 3221 (1998); M. A. Peterson and J. Ferry, Phys. Rev. A **39**, 2740 (1989); D. A. Kurtze, *ibid.* **43**, 7066 (1991); H. Sakaguchi, K. Kishinawa, K. Katsuki, and H. Honjo, Phys. Rev. E **75**, 021606 (2007).
[28] M. O. Bernard, J. Garnier, and J. F. Gouyet, Phys. Rev. E **64**, 041401 (2001).
[29] B. Shraiman and D. Bensimon, Phys. Rev. A **30**, 2840 (1984).
[30] R. C. Ball, Physica A **140**, 62 (1986).
[31] J. Szep and E. Lugosi, J. Phys. A **19**, L1109 (1986).
[32] M. B. Hastings and L. S. Levitov, Physica D **116**, 244 (1998).
[33] E. Somfai, R. C. Ball, J. P. DeVita, and L. M. Sander, Phys. Rev. E **68**, 020401(R) (2003); A. Taloni, E. Caglioti, V. Loreto, and L. Pietronero, J. Stat. Mech.: Theory Exp. (2006), P09004.
[34] C. J. G. Evertsz, P. W. Jones, and B. B. Mandelbrot, J. Phys. A **24**, 1889 (1991).
[35] W. Kager, B. Nienhuis, and L. P. Kadanoff, J. Stat. Phys. **115**, 805 (2004).